Enantiospecific Electrodeposition of Chiral CuO Films from Copper(II) Complexes of Tartaric and Amino Acids on Single-Crystal Au(001)

Hiten M. Kothari, Elizabeth A. Kulp, Sansanee Boonsalee, Maxim P. Nikiforov, Eric W. Bohannan, Philippe Poizot, Shuji Nakanishi, and Jay A. Switzer*

Department of Chemistry and Graduate Center for Materials Research, University of Missouri—Rolla, Rolla, Missouri 65409-1170

Received July 1, 2004. Revised Manuscript Received August 19, 2004

Chiral films of CuO were electrochemically deposited onto achiral Au(001) using chiral precursors such as tartaric acid and the amino acids alanine and valine to complex the Cu(II). The chirality of the electrodeposited films was dictated by the chiral solution precursor. X-ray diffraction pole figures and azimuthal scans, in conjunction with stereographic projections, were used to determine the absolute configuration and enantiomeric excess of the chiral CuO films. CuO films grown from L-tartaric acid have a $(1\bar{1}\bar{1})$ orientation with an enantiomeric excess of 95%, while the films grown from D-tartaric acid have a $(\bar{1}11)$ orientation with an enantiomeric excess of 93%. CuO films grown from chiral amino acids have two types of chiral orientations, each showing lower enantiomeric excess compared with the films deposited from tartaric acid. The films grown from L-alanine and L-valine solution have an excess of the $(\bar{1}11)$ and $(\bar{1}\bar{1}\bar{1})$ orientations, while the films grown from D-alanine and D-valine have an excess of $(1\bar{1}\bar{1})$ and (111). Films of CuO deposited from a solution of achiral glycine consist of a racemic mixture of the $(\bar{1}11)$ and $(1\bar{1}1)$ orientations. Chiral CuO films deposited on both single-crystal Au(001) and polycrystalline Au films were shown to exhibit chiral recognition for the electrochemical oxidation of tartaric acid.

Introduction

Chiral molecules are ubiquitous in the living world. Enantiomeric forms of chiral molecules differ from each other only in that they are nonsuperimposable mirror images of one another. Because one enantiomer may be useful while the other is toxic, the pharmaceutical industry is interested in devising processes to obtain enantiomerically pure forms of drugs and their precursors.[1] Traditionally, the industry has relied on using homogeneous solution-based catalysis or enzymatic reactions to carry out enantiospecific syntheses. Replacing homogeneous catalysts with heterogeneous catalysts could lead to improved process and cost efficiency.[2] Another use of enantiomeric surfaces would be to produce chiral sensors.

Efforts to develop enantiospecific heterogeneous catalytic systems have relied on breaking the symmetry of a metal surface by irreversibly adsorbing chiral molecules. A Raney Ni surface modified by adsorbing (*R,R*)-tartaric acid has been used to catalyze the hydrogenation of β-ketoesters, producing the *R*-product with over 90% enantiomeric excess (ee), while the surface modified with (*S,S*)-tartaric acid selectively produces the *S*-product.[3] Another example is the Orito[4] reaction, in which hydrogenation of α-ketoesters over alumina-supported platinum catalysts modified with chiral cinchonidine yields enantioselective products. Experimental and theoretical efforts to elucidate the mechanism for chiral recognition remain a topic of active research. Baiker[5] and McBreen[6] attribute the selectivity to a hydrogen bond between the chichonidine and ketoester, while Sun and Houk[7] suggest that the formation of a covalent bond between the amine group of the cinchonidine with the carbonyl group of the ketone gives the observed selectivity. Separation of chiral molecules using chromatographic techniques also relies on the extent of interaction between the enantiomeric forms with a chirally modified stationary phase.[8,9]

The durability of adsorbed modifiers is a serious concern for practical applications. An alternative to the adsorption approach would be to develop surfaces that are intrinsically chiral. McFadden et al.[10] proposed one such approach, where high index surfaces of fcc metals were shown to be chiral. They showed that even for a material with a highly symmetric space group, high

* To whom correspondence should be addressed. E-mail: jswitzer@umr.edu.

(1) Stinson, S. C. *Chem. Eng. News* **2001**, *79* (40), 79.
(2) Jacoby, M. *Chem. Eng. News* **2004**, *82* (11), 37.
(3) Izumi, Y. *Adv. Catal.* **1994**, *32*, 215.
(4) Orito, Y.; Imai, S.; Nyugen, G. *Synth. Org. Chem. Jpn.* **1979**, *37*, 173.
(5) Bonalumi, N.; Burgi, T.; Baiker, A. *J. Am. Chem. Soc.* **2003**, *125*, 13342.
(6) Lavoie, S.; Laliberte, A.-M.; McBreen, H. P. *J. Am. Chem. Soc.* **2003**, *125*, 15756.
(7) Vayner, G.; Houk, N. K.; Sun, K.-Y. *J. Am. Chem. Soc.* **2004**, *126*, 199.
(8) Armstrong, D. W.; Tang, Y.; Chen, S. *Anal. Chem.* **1994**, *66*, 1473.
(9) Armstrong, D. W.; Tang, Y.; Ward, T. *Anal. Chem.* **1993**, *65*, 1114.
(10) McFadden, C. F.; Cremer, P. S.; Gellman, A. J. *Langmuir* **1996**, *12*, 2483.

10.1021/cm048939x CCC: $27.50
Published on Web 10/05/2004

index surfaces could be chiral. The chirality is attributed to the presence of kink sites on these surfaces, and rules to identify and label these surfaces have been proposed.[11,12] Enantiospecific adsorption of chiral molecules on the Pt(643) surface was reported by Scholl et al.[13] using Monte Carlo simulations, while experimental evidence of chiral recognition was reported by Attard et al.,[11,14] who showed enantiospecific electrochemical oxidation of glucose in aqueous solutions on Pt(643) and Pt($\bar{6}4\bar{3}$)surfaces.

Our approach to the development of new chiral heterogeneous catalysts and sensors is to deposit chiral metal oxides films on achiral substrates. Recently, our group demonstrated that thin chiral films of CuO can be electrodeposited on Au(001)[15] and Cu(111)[16] single crystals using a simple and relatively inexpensive method. As is the case with fcc metals, it was observed that although the bulk crystal structure for CuO is centrosymmetric, the crystallographic orientation of the deposited film is chiral. The chirality of the electrodeposited film in the alkaline bath was determined by the enantiomer of tartrate used to complex Cu(II). Here we present details on the electrodeposition of chiral CuO films onto Au(001) from solutions using tartaric acid to direct the chirality. In particular, we show how X-ray diffraction pole figures and azimuthal scans can be used to determine the absolute configuration and enantiomeric excess of the chiral films. We also contrast these results to CuO films deposited onto Au(001) using Cu(II) complexes of the amino acids alanine, valine, and glycine as precursors.

Experimental Section

Electrochemical experiments were carried out using an EG&G Princeton Applied Research (PAR) model 273A potentiostat/galvanostat. The cell consisted of a platinum counter electrode and a standard calomel reference electrode (SCE). An Au(001) single-crystal purchased from Monocrystal Company (diameter 10 mm and thickness 2 mm) was used as a working electrode. A gold wire fitted around the single crystal served as an electrical contact to the working electrode. The working electrode was placed in solution using the meniscus method. The Au(001) single crystal was electropolished and annealed in a hydrogen flame prior to deposition. Electropolishing was carried out anodically, at a constant current density of 1.5 A/cm^2 in a moderately stirred solution of 50 vol % ethanol, 25 vol % ethylene glycol, and 25 vol % concentrated HCl at 55 °C.

Case 1: Deposition using Tartaric Acid. Thin films of CuO were deposited on Au(001) single crystals from an alkaline solution of copper(II) complexed with tartaric acid.[15,16,18] The concentrations in the deposition bath were 0.2 M Cu(II), 0.2 M tartaric acid, and 3 M NaOH. Films were deposited on the Au(001) single crystal at a constant anodic current density of 1 mA/cm^2 at 30 °C for 30 min giving an approximate thickness of 300 nm. L-Tartaric acid [(*R,R*)-(+)-tartaric acid], D-tartaric acid [(*S,S*)-(−)-tartaric acid] and DL-tartaric acid were purchased from Aldrich. The single enantiomers had an optical purity of ≥ 99% ee. The enantiomers were used without further purification.

Case 2: Deposition using Amino Acids. The solutions for deposition from amino acids were prepared by complexing Cu(II) with an excess of amino acid in base. The solution for depositing CuO from amino acids in this article was first reported by Ogura et al.,[17] and consisted of 50 mM amino acid, 5 mM Cu(II), and 0.2 M NaOH. The amino acids studied were achiral glycine and the L-, D-, and racemic forms of alanine and valine. Glycine with 98.5+% chemical purity was purchased from Aldrich. The L- and D-amino acids were purchased from Fluka and had ≥99.5% and ≥99% chemical purity, respectively. The racemic amino acid solutions were made using equal amounts of the L- and D-amino acids. Films were deposited on Au(001) single crystal at a constant anodic current density of 100 μA/cm^2 at 30 °C for 5 min.

X-ray Diffraction Measurements. X-ray diffraction measurements were performed with a high-resolution Philips X'Pert MRD diffractometer. For the Bragg−Brentano scan the primary optics module was a combination Göbel mirror and a 2-crystal Ge(220) 2-bounce hybrid monochromator, and the secondary optics module was a 0.18° parallel plate collimator. The hybrid monochromator produces pure Cu Kα_1 radiation (λ = 0.1540562 nm) with a divergence of 25 arc seconds. Pole figures were obtained in point-focus mode using a crossed-slit collimator as the primary optics and a flat graphite monochromator as the secondary optics. Stereographic projections were generated using Desktop Microscopy software (version 2.1) on an Apple Macintosh computer.

Electrochemical Selectivity. Electrochemical selectivity experiments to confirm the chirality of the electrodeposited CuO films were carried out in an aqueous solution of 0.1 M NaOH containing 5 mM L-tartaric acid or D-tartaric acid. The cyclic voltammograms (CV) were obtained in unstirred solutions at a scan rate of 10 mV/sec. The electrode was cleaned by scanning from the open circuit potential (OCP) to 0.75 V vs SCE in 0.1 M NaOH before changing solutions to remove remnants from the previous solution adsorbed on the electrode. The geometric area of the CuO film was controlled by mounting the electrode in a homemade Teflon holder.

Results and Discussion

CuO has a monoclinic structure with a centrosymmetric space group, *C*2/*c*.[19−21] Figure 1 shows two unit lengths of monoclinic CuO in each direction with red atoms representing Cu and gray atoms representing O. The figure shows that each Cu atom is coordinated to four O atoms to form a distorted square-planar geometry. A unit cell contains two Cu atoms, each coordinated to four oxygen atoms to form a parallelogram parallel to the [110] and [$\bar{1}$10] directions. Figure 1 shows the parallelogram along the [110] direction in light gray while the parallelogram parallel to the [$\bar{1}$10] direction is shown in dark gray. The Cu−O bond distances are 0.1959 and 0.1957 nm, and the O−Cu−O bond angles are 84.3° and 95.7°. Similarly, each O atom is coordinated to four Cu atoms resulting in a distorted tetrahedron (not shown in the figure). High-resolution powder diffraction studies on various CuO samples show broadening and asymmetry in peak shapes. The asymmetry has been attributed to nonstoichiometry due to cation vacancies, possibly resulting in the change of bond length or angle.[20] In a recent high-resolution X-ray

(11) Attard, G. A. *J. Phys. Chem. B* **2001**, *105*, 3158.
(12) Scholl, D. S.; Asthagiri, A.; Power, T. D. *J. Phys. Chem. B* **2001**, *105*, 4771.
(13) Scholl, D. S. *Langmuir* **1998**, *14*, 862.
(14) Ahmadi, A.; Attard, G.; Feliu, J.; Rodes, A. *Langmuir* **1999**, *15*, 2420.
(15) Switzer, J. A.; Kothari, H. M.; Poizot, P., Nakanishi, S.; Bohannan, E. W. *Nature* **2003**, *425*, 490.
(16) Bohannan, E. W.; Kothari, H. M.; Nicic, I. M.; Switzer, J. A. *J. Am. Chem. Soc.* **2004**, *126*, 488.
(17) Nakaoka, K.; Ogura, K. *J. Electrochem. Soc.* **2002**, *149*, C579.
(18) Poizot, P.; Hung, C.-J.; Nikiforov, M. P.; Bohannan, E. W.; Switzer, J. A. *Electrochem. Solid-State Lett.* **2003**, *6*, C21.
(19) Åsbrink, S.; Norrby L.-J. *Acta Crystallogr.* **1970**, *B26*, 8.
(20) Langford, J. I.; Louër, D. *J. Appl. Crystallogr.* **1991**, *24*, 149.
(21) Brese, N. E.; O'Keefe, M.; Ramakrishna, B. L.; Von Dreele, R. B. *J. Solid State Chem.* **1990**, *89*, 184.

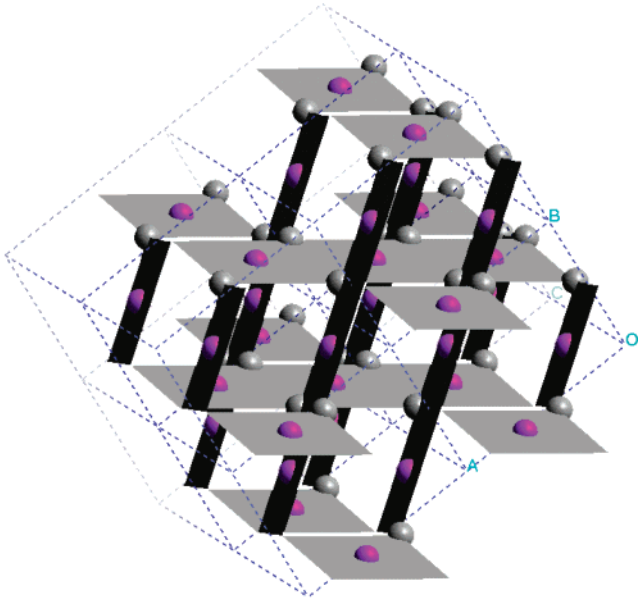

Figure 1. Structure of monoclinic CuO with space group *C*2/*c*. The Cu atoms are shown in red, and the O atoms are shown in gray. The planes in light gray and dark gray show the Cu coordination with nearest O atoms along the [110] and [$\bar{1}$10] directions, respectively.

diffraction study on single-crystal CuO by Åsbrink,[22] the pattern is better fit by the noncentrosymmetric space group *Cc*.[22] The contrast is attributed to a more stoichiometric CuO having less cation deficiencies. Consistent with previous reports from our group and other studies on CuO, the centrosymmetric space group, *C*2/*c* is used for generating the stereographic projections to explain the pole figures.

Epitaxial films of CuO have been reported on MgO substrates under high vacuum and high-temperature conditions using MBE[23] and MOCVD.[24] Polycrystalline films of CuO have been electrodeposited at room temperature on Au and Pt in alkaline solution using amino acids[17] to complex the Cu(II). Our group has previously reported electrodeposition of CuO on polycrystalline substrates using L-tartaric acid[18] as a complexing agent. We measured lattice parameters for CuO powder obtained from several films using Rietveld analysis with space group *C*2/*c*. The values reported were $a = 0.4685$ nm, $b = 0.3430$ nm, $c = 0.5139$ nm, $\beta = 99.08°$, and $\alpha = \gamma = 90°$. The thickness of the film deposited for 1200 s at 1 mA/cm^2 calculated by monitoring the frequency change on the Au electrochemical quartz crystal microbalance (EQCM) electrode (area = 0.2 cm^2) as a function of time is 180 nm. The thickness measured by the EQCM matches the thickness of 200 nm obtained from a cross-sectional SEM image on the same electrode. In the EQCM measurement, the plot of frequency change vs time is linear indicating that the deposited film does not inhibit further film formation. Since the number of electrons involved in the reaction is not known, no estimate of the current efficiency was determined.

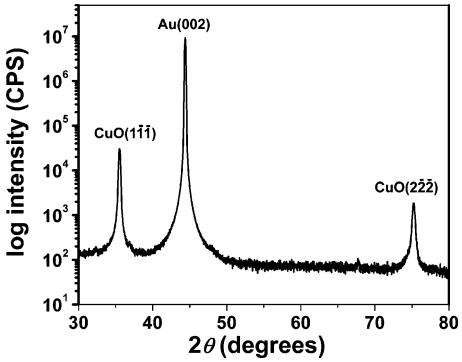

Figure 2. X-ray diffraction $\theta-2\theta$ scan for a 300- nm-thick CuO film deposited on Au(001) from a solution of L-tartaric acid. Only the {1$\bar{1}\bar{1}$} planes are evident in the figure, indicating that the system has a CuO(1$\bar{1}\bar{1}$)//Au(001) epitaxial relationship.

Table 1. List of Planes Having Identical *d* Spacing for Monoclinic CuO

2θ (degrees)	*d*-spacing (nm)	planes
35.570	0.25246	(1$\bar{1}\bar{1}$), ($\bar{1}$11), (11$\bar{1}$), ($\bar{1}\bar{1}$1)
38.742	0.23223	(111), ($\bar{1}\bar{1}\bar{1}$), (1$\bar{1}$1), ($\bar{1}$1$\bar{1}$)

Figure 2 shows a $\theta-2\theta$ X-ray diffraction scan for a 300 nm CuO film deposited on Au(001) at an anodic current density of 1 mA/cm^2 for 1800 s at 30 °C from a solution of Cu(II) complexed with L-tartaric acid. $\theta-2\theta$ X-ray diffraction scans probe the orientation of the film perpendicular to the substrate. Only the {1$\bar{1}\bar{1}$} set of peaks is seen in the figure indicating the presence of a (1$\bar{1}\bar{1}$) texture for the electrodeposited film. The results obtained here represent diffraction from the entire volume of the film and not just the surface. The CuO film in Figure 2 has a strong peak at $2\theta = 35.57°$ ($d = 0.2525$ nm). Table 1 lists the set of planes that have the same *d*-spacings. Based on the listings in Table 1, the peak in the X-ray scan could be assigned as any one of the four orientations. The (1$\bar{1}\bar{1}$), ($\bar{1}$11), (11$\bar{1}$), and ($\bar{1}\bar{1}$1) planes have identical *d*-spacing of 0.2525 nm and it is impossible to distinguish between the orientations based on the $\theta-2\theta$ scans. The orientations can be assigned with the help of X-ray diffraction pole figures and stereographic projections. As discussed later, the films grown from a solution of L-tartaric acid have a {1$\bar{1}\bar{1}$} out of plane orientation, i.e., CuO(1$\bar{1}\bar{1}$)//Au(001). Similar scans obtained for a film deposited from a solution of Cu(II) complexed with D-tartaric acid have a {$\bar{1}$11} out of plane orientation, i.e., CuO($\bar{1}$11)//Au(001).

Figure 3a and b show the (1$\bar{1}\bar{1}$) and ($\bar{1}$11) stereographic projections of monoclinic CuO. A stereographic projection is a two-dimensional graphical representation of the crystal symmetry and the interplanar angles. The radial direction is the tilt angle, χ, of the sample, while the azimuthal angle, ϕ, is the rotation of the sample about its axis. The positions of CuO{111} planes are specified. In addition, the positions of CuO{100} are also specified because the CuO(200) *d*-spacing is similar to the CuO(111) *d*-spacing, and reflections from the CuO-(100) planes will be simultaneously observed in a CuO-(111) pole figure. Clearly evident is that the two images are nonsuperimposable mirror images. Figure 3a shows that for the (1$\bar{1}\bar{1}$) orientation, reflections from the (1$\bar{1}$1) plane at a tilt angle, χ, of 57°, and the ($\bar{1}\bar{1}\bar{1}$) plane at tilt angle, χ, of 63°, are separated azimuthally by 115°

(22) Åsbrink, S.; Waśkowska, A. *J. Phys.: Condens. Matter* **1991**, *3*, 8173.
(23) Catana, A.; Locquet, J.-P.; Paik, S. M.; Schuller, I. K. *Phys. Rev. B* **1992**, *46*, 15477.
(24) Watson, I. M.; Atwood, M. P.; Cumberbatch, T. J. *Thin Solid Films* **1994**, *251*, 51.

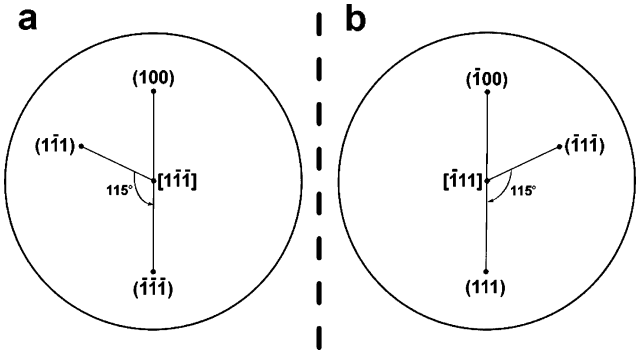

Figure 3. Stereographic projections for (a) (1$\bar{1}\bar{1}$) and (b) ($\bar{1}$11) orientations indicating the positions where the (111)-type and the (100)-type reflections should be observed in the pole figures. The (100) and ($\bar{1}$00) reflections are shown, as the CuO(200) *d*-spacing is similar to the CuO(111) *d*-spacing, and reflections from the CuO(100) planes will be observed in a CuO(111) pole figure. For the (1$\bar{1}\bar{1}$) orientation, reflections from the (1$\bar{1}$1) plane at $\chi = 57°$ and the (1$\bar{1}\bar{1}$) plane at $\chi = 63°$ are separated azimuthally by 115° rotated counterclockwise. For the ($\bar{1}$11) orientation, reflections from ($\bar{1}$1$\bar{1}$) plane at $\chi = 57°$ and (111) plane at $\chi = 63°$ are separated azimuthally by 115° rotated clockwise.

Table 2. Calculated Interplanar Angles, χ, between the Observed Orientation in the $\theta-2\theta$ X-ray Diffraction Scans and the CuO Reflections Being Probed in the Pole Figure

plane 1	plane 2	χ (deg)
(1$\bar{1}\bar{1}$)	($\bar{1}\bar{1}$1)	62.93
(1$\bar{1}\bar{1}$)	(1$\bar{1}$1)	56.92
(1$\bar{1}\bar{1}$)	(100)	62.44
($\bar{1}$11)	(111)	62.93
($\bar{1}$11)	($\bar{1}$1$\bar{1}$)	56.92
($\bar{1}$11)	($\bar{1}$00)	62.44

rotated counterclockwise ($\Delta\phi = -115°$). Figure 3b shows that for the ($\bar{1}$11) orientation, reflections from the ($\bar{1}$1$\bar{1}$) plane at $\chi = 57°$ and the (111) plane at $\chi = 63°$ are separated azimuthally by 115° rotated clockwise ($\Delta\phi = +115°$). The calculated interplanar angles for these planes of interest are summarized in Table 2. Figure 3 shows that although the (1$\bar{1}\bar{1}$) and the ($\bar{1}$11) planes have identical *d*-spacings they are not really equivalent in the sense that the mirror images of their stereographic projections are not superimposable. Analyzing the stereographic projections for the other two planes, (11$\bar{1}$) and ($\bar{1}$1$\bar{1}$), and comparing them with the stereographic projections of (1$\bar{1}\bar{1}$) and ($\bar{1}$11) shows that CuO($\bar{1}$11) and CuO(11$\bar{1}$) are equivalent and CuO(1$\bar{1}\bar{1}$) and CuO($\bar{1}\bar{1}$1) are equivalent.

The in-plane orientation, or the orientation of the film parallel with the substrate, is confirmed by running X-ray diffraction pole figures. For chiral films, the X-ray pole figures can be used to determine the absolute configuration of the film. Pole figures are obtained by selecting a reflection to probe while measuring the diffracted intensity as a function of sample tilt (χ) and rotation (ϕ). The sample is tilted from $\chi = 0°$ to 90° and for each tilt angle the sample is rotated through azimuthal angles, ϕ, of 0° to 360°. Generally, a reflection with highest intensity for a randomly oriented powder is probed to achieve high diffracted intensity. The (111) plane with $2\theta = 38.742°$ ($d = 0.23223$ nm) has the highest intensity for polycrystalline CuO and was probed in the pole figures. As discussed later in the text, the added advantage of using the (111)-pole figure is that it provides an internal reference in the form of Au(111) reflections for comparing different pole figures.

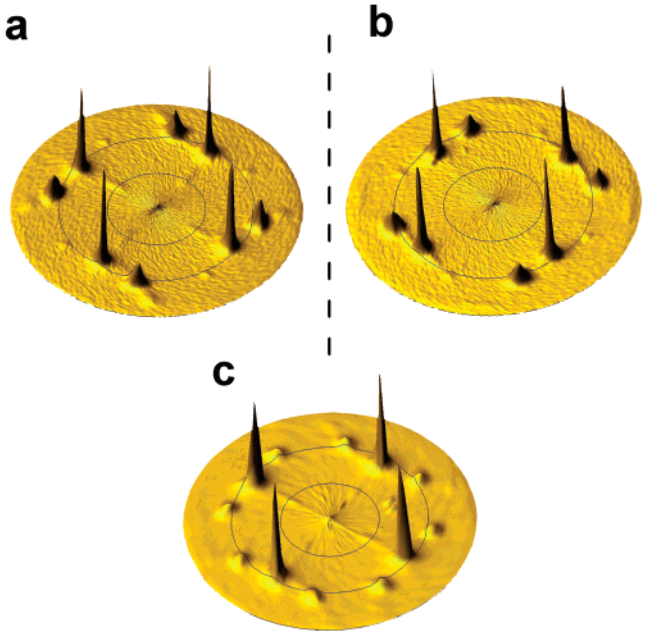

Figure 4. CuO(111) pole figures for films of CuO on Au(001) grown from solutions of (a) L-tartaric acid, (b) D-tartaric acid, and (c) DL-tartaric acid. The film grown from L-tartaric acid has a (1$\bar{1}\bar{1}$) orientation while the film grown from D-tartaric acid has a ($\bar{1}$11) orientation. The film deposited from the racemic mixtures has equal amounts of the (1$\bar{1}\bar{1}$) and ($\bar{1}$11) orientations.

Figure 4 shows (111) pole figures for 300 nm thick CuO films deposited on Au(001) from a solution of (a) L-tartaric acid, (b) D-tartaric acid, and (c) DL-tartaric acid. The radial direction is the tilt of the sample with the grid lines in the figure spaced 30° apart. The *d*-spacing of CuO(111) is very close to the *d*-spacing of Au(111), which results in the reflection of Au(111) peaks in the same pole figure. Similarly, the *d*-spacing of CuO(200) is very close to the *d*-spacing of CuO(111), so reflections from the CuO(100) planes should also be evident in the same pole figure. Although the 2θ is maximized to observe the reflection from CuO(111) planes, the final pole figure is actually a superposition of the CuO(111), Au(111), and CuO(100) pole figures.

The interplanar angle between the (100) and (111) planes in a cubic system is 54.7°. Thus, the four intense peaks at approximately $\chi = 55°$ result from the {111} reflections of Au. The Au{111} reflections at $\chi = 55°$, spaced 90° apart azimuthally, are much more intense than the corresponding CuO{111} reflections at $\chi = 57°$. The peaks at $\chi = 63°$ are due to the CuO{111} and CuO{100} planes. Since the (111)-type planes of CuO and Au overlap we conclude that CuO deposits without rotation on the Au surface. The epitaxial relationship consistent with this observation is CuO[110]//Au[110]. While the X-ray results do not provide information on the structure of the CuO−Au interface, they do determine the orientation of the bulk film with respect to the substrate. If only one domain of CuO was deposited, then only three peaks would be observed in the pole figure. The CuO(1$\bar{1}$1) peak would be obscured by the Au(111) peak at $\chi = 55°$ while the intense CuO($\bar{1}\bar{1}\bar{1}$) peak and the less intense CuO(100) peak would be

observed opposite one another at $\chi = 63°$. The presence of four peaks of equal intensity at $\chi = 63°$ in Figure 4a and b at $\Delta\phi = 90°$ shows that there are four equivalent in-plane orientations, with the [110] direction of CuO coincident with the [110], [1$\bar{1}$0], [$\bar{1}$10], and [$\bar{1}\bar{1}$0] directions of Au. This is reasonable because the Au(001) surface is 4-fold symmetric. The presence of four different domains was cross-checked by running CuO(20$\bar{2}$) pole figures.

On the basis of the above analyses we can conclude that the film grown in L-tartaric acid has a CuO(1$\bar{1}\bar{1}$) or CuO($\bar{1}$1$\bar{1}$) orientation. We arbitrarily assign it as CuO(1$\bar{1}\bar{1}$). Similarly the film grown in D-tartaric acid has a CuO($\bar{1}$11) or CuO(11$\bar{1}$) orientation. The film is assigned a CuO($\bar{1}$11) orientation. In our previous reports,[15,16] L-tartaric acid was incorrectly identified as (*S,S*)-(−)-tartaric acid while D-tartaric acid was incorrectly identified as (*R,R*)-(+)tartaric acid. Thus, although the pole figures were correctly analyzed, the assignment of CuO orientations to the solution precursors should be reversed. The mistake with the nomenclature is rectified in this report. The films grown from L-tartaric acid [(*R,R*)-(+)-tartaric acid] have a CuO(1$\bar{1}\bar{1}$) orientation while the films grown from D-tartaric acid [(*S,S*)-(−)-tartaric acid] have a CuO($\bar{1}$11) orientation. With the intense Au peaks at $\chi = 55°$ acting as an internal reference it is evident that Figure 4a and b are nonsuperimposable mirror images of each other. Therefore, the two orientations are enantiomorphs. Figure 4c shows that the film grown from a racemic mixture of tartaric acid has equal amounts of two enantiomeric orientations. This can be quantified in terms of the enantiomeric excess of one orientation with respect to the other.

The enantiomeric excess of one orientation over the other can be determined from azimuthal scans probing the CuO (111)-type reflections at $\chi = 63°$. Figure 5 shows the azimuthal scans extracted from the (111) pole figures at $\chi = 63°$ with the azimuthal angle, φ, varying from 60° to 120°. Figure 5a shows the scan for a film deposited from L-tartaric acid solution having a preferred (1$\bar{1}\bar{1}$) orientation. Figure 5b shows the scan for a film deposited from D-tartaric acid solution having a preferred ($\bar{1}$11) orientation. Figure 5c shows that the film from DL-tartaric acid has an equal amount of both orientations. The peaks in blue and red represent ($\bar{1}\bar{1}\bar{1}$) and (111) reflections, respectively. The film grown from L-tartaric acid has a higher diffracted intensity for ($\bar{1}\bar{1}\bar{1}$) reflection while the film grown from D-tartaric acid has a higher diffracted intensity for (111) reflection. The film deposited from the racemic mixtures has approximately equal intensity for the ($\bar{1}\bar{1}\bar{1}$) and (111) reflections. The percentage enantiomeric excess for the (1$\bar{1}\bar{1}$) orientation can be calculated quantitatively from the area under all the peaks obtained at $\chi = 63°$ using the formula

$$ee = \left(\frac{A_{(1\bar{1}\bar{1})} - A_{(\bar{1}11)}}{A_{(1\bar{1}\bar{1})} + A_{(\bar{1}11)}}\right) \times 100$$

The film deposited from L-tartaric acid has an enantiometric excess of 95% while the film deposited from D-tartaric acid has an enantiometric excess of 93%. The film from DL-tartaric acid has equal amounts of both orientations and has essentially zero enantiomeric excess. Also evident in the scans is the low background intensity. The peak-to-background ratio of the measured intensities ($I_{peak}/I_{background}$) in the azimuthal scans is a good indicator of the nature of the epitaxy. A material with a fiber texture has an $I_{peak}/I_{background}$ of unity. The films grown from solutions of L-tartaric acid and D-tartaric acid have $I_{peak}/I_{background}$ ratios of 92 and 99, respectively. The film grown from solution of DL-tartaric acid has an $I_{peak}/I_{background}$ ratio of 56.

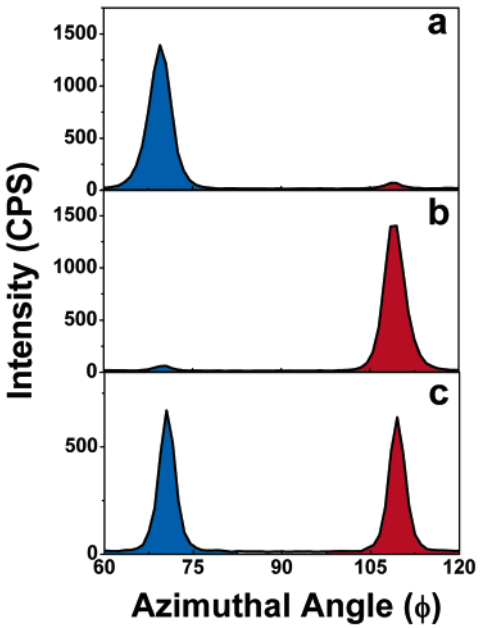

Figure 5. Azimuthal scans probing the {111} reflections at $\chi = 63°$ for films of CuO on Au(001) grown from solutions of (a) L-tartaric acid, (b) D-tartaric acid, and (c) DL-tartaric acid. The peaks in blue and red represent the ($\bar{1}\bar{1}\bar{1}$) and (111) reflections, respectively. The film grown from L-tartaric acid has a higher diffracted intensity for the ($\bar{1}\bar{1}\bar{1}$) reflection (ee = 95%), while the film grown from D-tartaric acid has a higher diffracted intensity for the (111) reflection (ee = 93%). The film deposited from the racemic mixture has approximately equal intensities for the ($\bar{1}\bar{1}\bar{1}$) and (111) reflections (ee = 0%).

Figure 6 shows polyhedral models for CuO when the (1$\bar{1}\bar{1}$) and ($\bar{1}$11) planes are oriented parallel to the plane of the paper. This figure illustrates that the two faces are nonsuperimposable mirror images of each other. That is, the two planes are chiral. The Cu atoms are represented in red and the oxygen atoms are represented in gray. Although CuO has an achiral space group, the (1$\bar{1}\bar{1}$) and ($\bar{1}$11) faces are enantiomorphs because they lack mirror symmetry.

We have not been able to correlate the handedness of the electrodeposited films with their microstructure, as observed by scanning electron microscopy (SEM). Figure 7 shows the SEM images of films grown from L-tartaric acid, D-tartaric acid, and DL-tartaric acid. All the images show a crosshatch pattern on the surface, with crystallites that are approximately 100 nm long and 25 nm wide. The individual crystallites have a rice grain structure, but multiple domains of each orientation rotated 90° result in the crosshatch morphology. The SEM images of films from D-tartaric acid and L-tartaric acid are similar, while the DL-tartaric acid film, in addition to the crosshatch features, shows larger globular features which could result from the grains of two different orientations growing together.

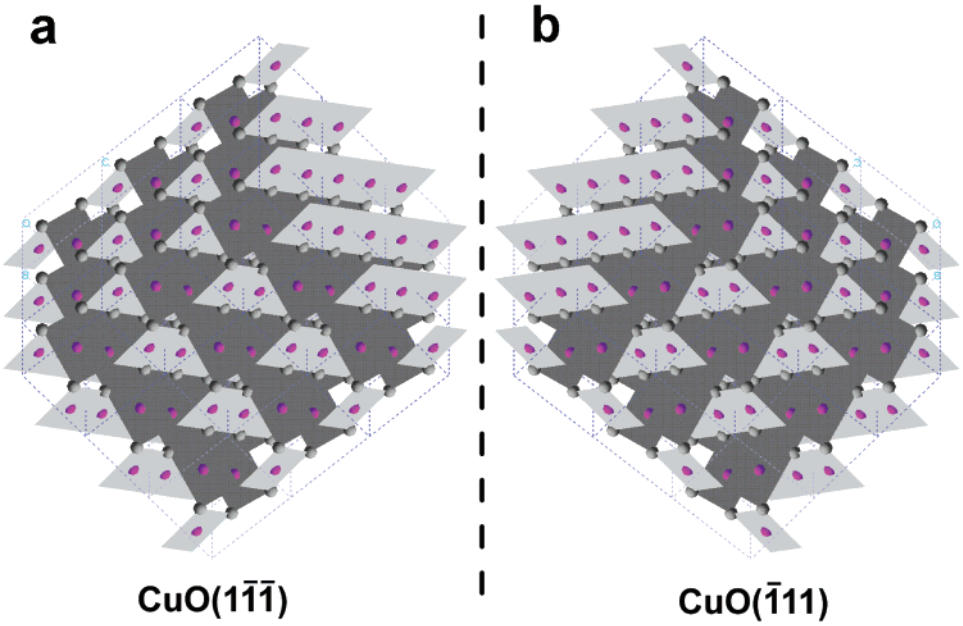

Figure 6. Polyhedral models for the (1$\bar{1}\bar{1}$) and ($\bar{1}$11) orientations with the faces aligned parallel with the plane of the paper. The Cu atoms are shown in red, and the O atoms are shown in gray. The planes in light gray and dark gray show the Cu coordination with nearest O atoms along the [110] and [$\bar{1}$10] directions, respectively.

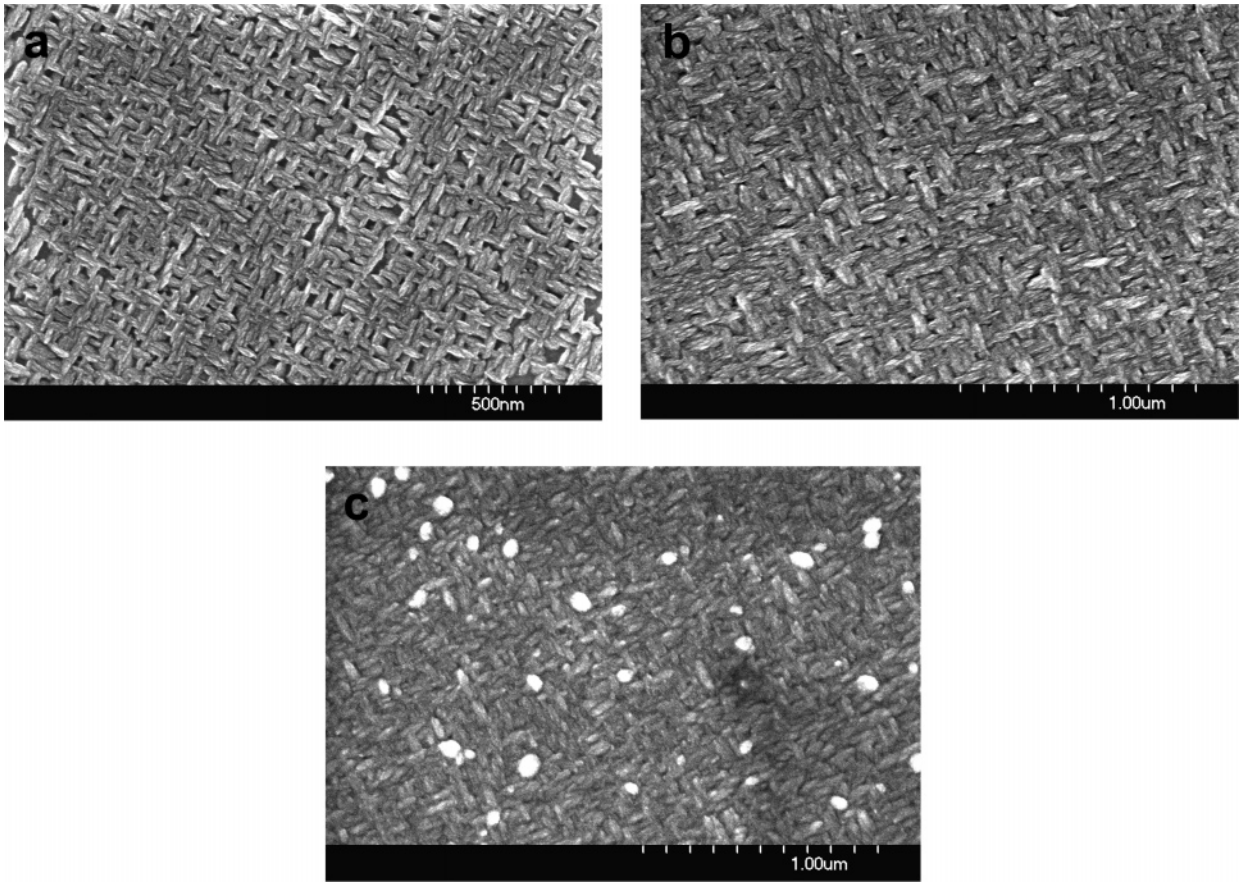

Figure 7. SEM images of CuO films on Au(001) grown from solutions of (a) L-tartaric acid, (b) D-tartaric acid, and (c) DL-tartaric acid

Organic additives are known to influence the morphology of the electrodeposited films.[25−27] We have previously shown that varying the solution pH and deposition potential controls the texture of electrodeposited Cu_2O films. Polycrystalline Cu_2O films grown from a Cu(II)−lactate complex show a preferred [100]

(25) Budevski, E.; Staikov, W.; Lorentz, W. J. *Electrochemical Phase Formation and Growth*; VCH: New York, 1996.

(26) Spyrellis, N.; Amblard, J.; Froment, M.; Maurin, G. *J. Microsc. Spectrosc. Electron.* **1987**, *12*, 220.

(27) Paunovic, M.; Schlesinger, M. *Fundamentals of Electrochemical Deposition*; Wiley-Interscience: New York, 1998; pp 167−186.

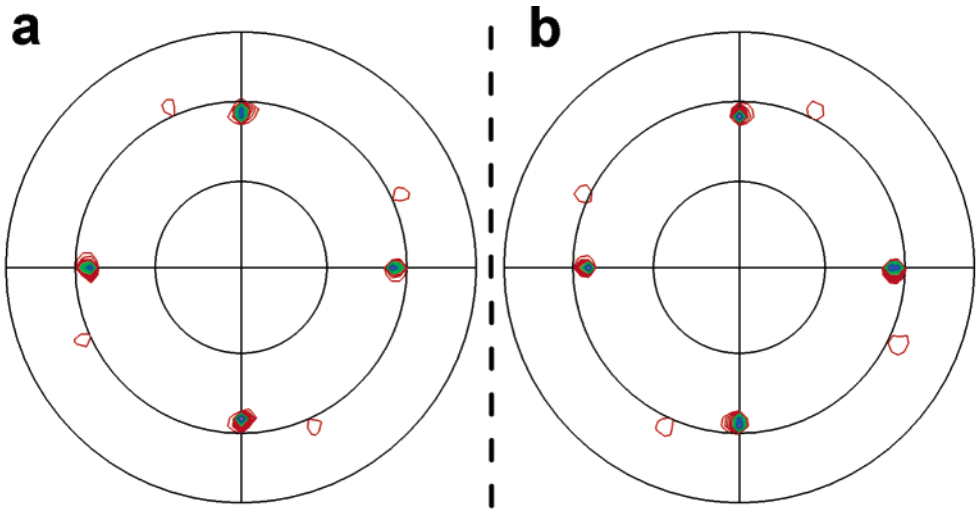

Figure 8. CuO(111) pole figures for films deposited on Au(001) from (a) L-tartaric acid for 30 min then D-tartaric acid for 30 min, and (b) D-tartaric acid for 30 min then L-tartaric acid for 30 min.

orientation at pH 9 whereas the preferred orientation changes to [111] at pH 12.[28] Epitaxial Cu_2O films grown on Au(001)[29] and InP(001)[30] at pH 12 undergo a thermodynamic to kinetic transition as a function of deposition potential. Films grown at low overpotentials follow the orientation of the substrate, but they undergo a transition to a kinetically controlled orientation when deposited at high overpotentials. In the present work, we show that the orientation and hence the chirality of the deposited film can be controlled at the molecular level by choosing the complexing agent used to prepare the solution. The handedness of the film is directed by the chirality of the deposition solution. The Au(001) surface is highly symmetric and does not impart chirality to the film.

Organic additives are also known to cause face-selective crystallization of inorganic crystals in biosystems.[31−35] Biomineralization studies have shown the selective nucleation of inorganic biominerals to be caused by the geometric matching, electrostatic interactions, and stereochemistry or a combination of these variables at the organic−inorganic interface.[32] Aizenberg et al., in recent studies of calcite nucleation on patterned self-assembled monolayers of alkanethiols on Au and Ag, have shown controlled calcite nucleation dependent on the surface termination of the thiol group.[34,35] In the presence of chiral amino acids, Cody crystallized asymmetric crystals of gypsum even though the space group of gypsum is symmetric. Changing the solution precursor systematically changed the handedness of the crystallites.[33] In related studies, Tend[36] and Orme[37] recently crystallized chiral single crystals of calcite using chiral aspartic acid in the solution. They also observed the formation of chiral etch pits during calcite dissolution in the presence of aspartic acid. Changes in step-edge free energies of the crystallized nuclei are suggested as a possible cause for the observed asymmetry.

Chirality can be bestowed on the surface by templating or by imprinting.[38] Chiral imprinting results when the adsorbed chiral molecule irreversibly reconstructs the substrate. The chirality of the substrate will remain intact on removal of the adsorbed molecule.[39,40] Chiral templating is induced by adsorbing chiral molecules on achiral surfaces without surface reconstruction. Adsorption of chiral tartaric acid on low index surfaces on Cu[41] and Ni[42] has been shown to break the symmetry of the underlying substrates. Raval et al. have shown that the adsorption of (*R*, *R*)-tartaric acid on Cu(110) surface creates long range order through chiral channels or holes across the Cu surface. The holes or channels lead the incoming molecules to bind with the underlying Cu atoms in a nonrandom stereo-geometry, subsequently aiding the formation of enantioselective products. No reconstruction of the underlying Cu atoms was evident. In contrast to the results on Cu(110), the same group showed that the adsorption of (*R*, *R*)-tartaric acid bestows chirality to the Ni(110) surface by causing extended chiral reconstruction of the underlying Ni(110) substrate.

In our case of electrodeposited chiral CuO films, it is reasonable to expect tartaric acid or copper−tartrate[43] complexes to adsorb on the Au(001) surface and break its symmetry. Complexes of Cu(II)−tartrate have a dimeric structure with a symmetry that is determined

(28) Golden, T. D.; Shumsky, M. G.; Zhou, G.-Y.; VanderWerf, R. A.; Van Leeuwen, R. A.; Switzer, J. A. *Chem. Mater.* **1996**, *8*, 2499.
(29) Switzer, J. A.; Kothari, H. M.; Bohannan, E. W. *J. Phys. Chem. B* **2002**, *106*, 4027.
(30) Liu, R.; Oba, F.; Bohannan, E. W.; Ernst, F.; Switzer, J. A. *Chem. Mater.* **2003**, *15*, 4882.
(31) Addadi, L.; Weiner, S. *Proc. Natl. Acad. Sci. U.S.A.* **1985**, *82*, 4110.
(32) Mann, S.; Archibald, A. D.; Didymus, J. M.; Douglas, T.; Heywood, B. R.; Meldrum, F. C.; Reeves, N. J. *Science* **1993**, *261*, 1286.
(33) Cody, A. M.; Cody, R. D. *J. Cryst. Growth* **1991**, *113*, 508.
(34) Aizenberg, J.; Black, A. J.; Whitesides, G. M. *J. Am. Chem. Soc.* **1999**, *121*, 4500.
(35) Aizenberg, J.; Black, A. J.; Whitesides, G. M. *Nature* **1999**, *398*, 495.
(36) Teng, H. H.; Dove, P. M.; Orme, C. A.; DeYoreo, J. J. *Science* **1998**, *282*, 724.
(37) Orme, C. A.; Noy, A.; Wierzbicki, A.; McBribge, M. T.; Grantham, M.; Teng, H. H.; Dove, P. M.; DeYoreo, J. J. *Nature* **2001**, *411*, 775.
(38) Hovrath J. D.; Gellman, A. J. *Top. Catal.* **2003**, *25*, 9.
(39) Zhao, X. *J. Am. Chem. Soc.* **2000**, *122*, 12584.
(40) Schunack, M.; Laegsgaard, E.; Stensgaard, I.; Johannsen, I.; Besenbacher, F. *Angew. Chem., Int. Ed.* **2001**, *40*, 2623.
(41) Lorenzo, M. O.; Badelley, C. J.; Muryn, C.; Raval, R. *Nature* **2000**, *404*, 376.
(42) Humblot, V.; Haq, S.; Muryn, C.; Hofer, W. A.; Raval, R. *J. Am. Chem. Soc.* **2002**, *124*, 503.
(43) Missavage, R. J.; Belford, R. L.; Paul, I. C. *J. Coord. Chem.* **1972**, *2*, 145.

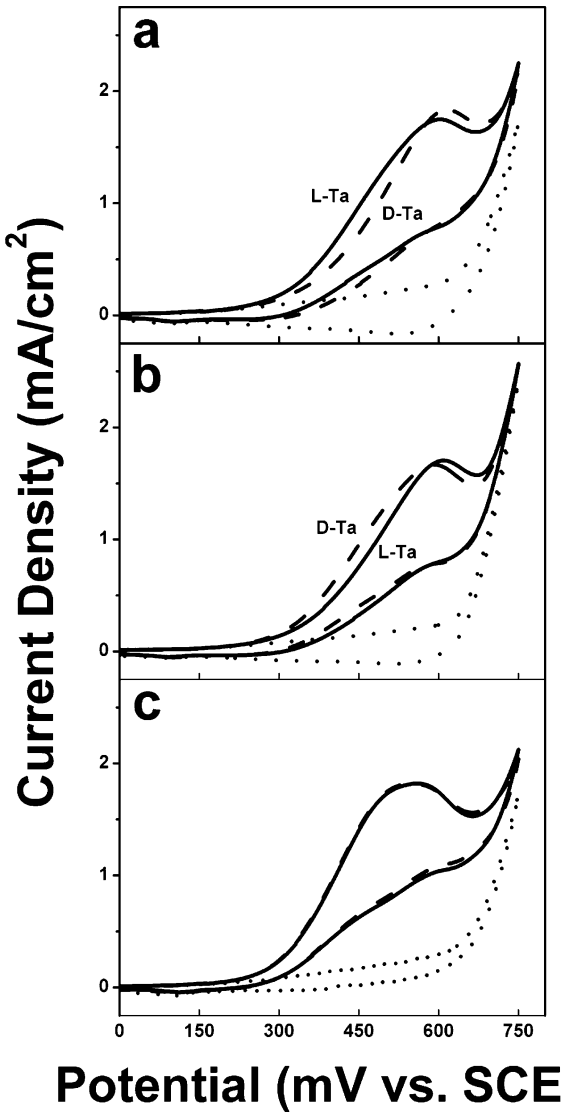

Figure 9. Chiral recognition of tartaric acid by chiral CuO deposited on Au(001). Cyclic voltammograms were run at room temperature in solutions of 5 mM L-tartaric acid (solid line) or 5 mM D-tartaric acid (dash) in 0.1 M NaOH (dot) for CuO films grown in (a) L-tartaric acid, (b) D-tartaric acid, and (c) DL-tartaric acid solutions. The film grown from L-tartaric acid selectively oxidizes L-tartaric acid over D-tartaric acid while the film grown from D-tartaric acid selectively oxidizes D-tartaric acid over L-tartaric acid. The control experiment in part (c) on an achiral film shows no selectivity for the electrooxidation of tartaric acid.

by the handedness of the tartrate ligand.[43] In our previous reports, the asymmetry has been attributed to the adsorption of chiral moieties such as free tartrate ion or Cu(II) tartrate complexes on the Au(001) surface. Surface reconstruction of the underlying Au substrate from the adsorbed molecules could be another cause for the asymmetry. The precise mechanism, however, is not known at this time. The presence of chiral modifiers is, however, necessary for the nucleation of chiral CuO domains. Once the film growth is initiated, the system is able to maintain the orientation regardless of the solution precursor. This is evident from the results in Figure 8. Here, a thin film of CuO was first deposited from a solution of L-tartaric acid for 30 min at 1 mA/cm^2. The film was grown thick enough to obtain a uniform deposit across the surface and eliminate any

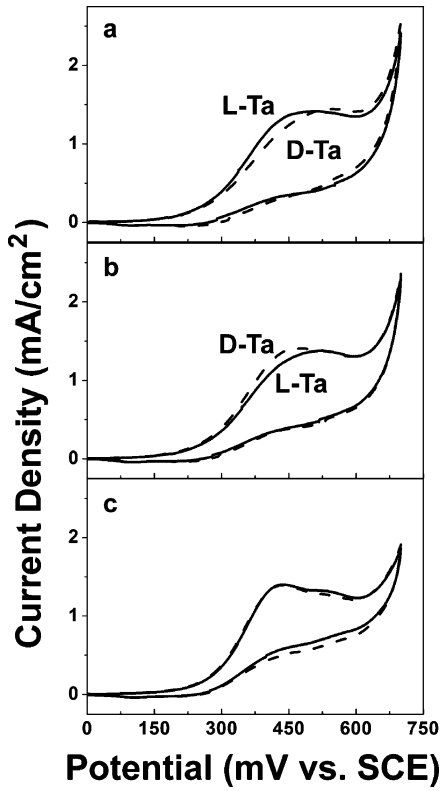

Figure 10. Chiral recognition of tartaric acid by chiral CuO deposited on a polycrystalline Au electrode. Cyclic voltammograms were run at room temperature in solutions of 5 mM L-tartaric acid (solid line) or 5 mM D-tartaric acid (dash) in 0.1 M NaOH for CuO films grown in (a) L-tartaric acid, (b) D-tartaric acid, and (c) DL-tartaric acid solutions. The film grown from L-tartaric acid selectively oxidizes L-tartaric acid over D-tartaric acid while the film grown from D-tartaric acid selectively oxidizes D-tartaric acid over L-tartaric acid. The control experiment in part (c) on an achiral film shows no selectivity for the electrooxidation of tartaric acid.

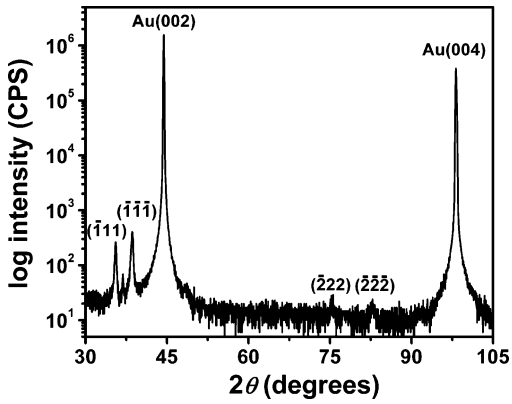

Figure 11. X-ray diffraction $\theta-2\theta$ scan of a CuO film on Au(001) from L-alanine solution. The unlabeled peak is due to a gold impurity.

substrate influence on subsequent deposit. Following the initial growth, the same electrode was used to grow a thicker film from the D-tartaric acid solution under similar deposition conditions for 30 min. Only the peaks from the CuO($1\bar{1}\bar{1}$) orientation are evident in the pole figure shown in Figure 8a. The pole figure and the orientation are identical to the results shown in Figure 4a. Similarly, the film grown from D-tartaric acid continues to grow with $\{\bar{1}11\}$ orientation after switching the deposition bath, as evident in Figure 8b.

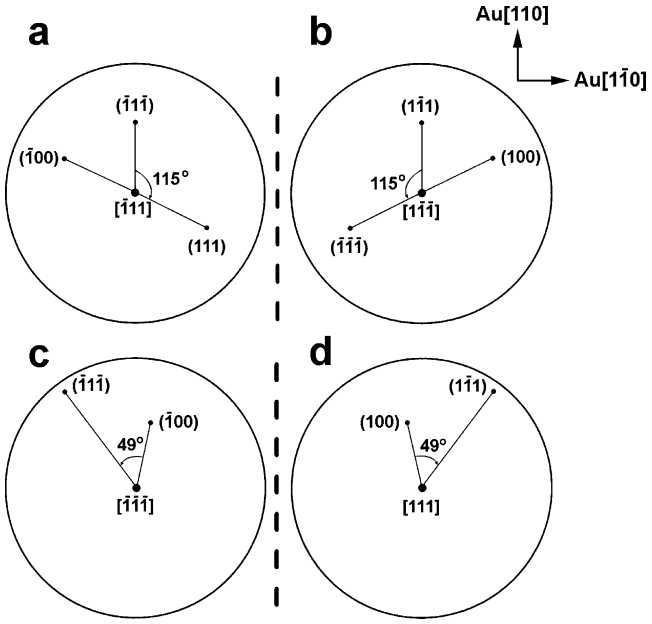

Figure 12. Stereographic projections for (a) ($\bar{1}$11), (b) (1$\bar{1}\bar{1}$), (c) ($\bar{1}\bar{1}\bar{1}$), and (d) (111) orientations indicating the positions where the (111)-type and (100)-type reflections should be observed in the pole figures. For the (1$\bar{1}\bar{1}$) orientation, reflections from the (1$\bar{1}$1) plane at $\chi = 57°$ and the ($\bar{1}\bar{1}\bar{1}$) plane at $\chi = 63°$ are separated azimuthally by 115° rotated counterclockwise. For the ($\bar{1}$11) orientation, reflections from the ($\bar{1}$1$\bar{1}$) plane at $\chi = 57°$ and the (111) plane at $\chi = 63°$ are separated azimuthally by 115° rotated clockwise. For the ($\bar{1}\bar{1}\bar{1}$) orientation, reflections from the ($\bar{1}$00) plane at $\chi = 55°$ and the ($\bar{1}\bar{1}$1) plane at $\chi = 85°$ are separated azimuthally by 49° rotated counterclockwise. For the (111) orientation, reflections from the (100) plane at $\chi = 55°$ and the (1$\bar{1}$1) plane at $\chi = 85°$ are separated azimuthally by 49° rotated clockwise. The Au directions are given as a reference.

Table 3. Calculated Interplanar Angles between the Observed Orientation in the $\theta-2\theta$ X-ray Diffraction Scans and the CuO Reflections Being Probed in the Pole Figure

plane 1	plane 2	χ (deg)	plane 1	plane 2	χ (deg)
($\bar{1}$11)	(11$\bar{1}$)	62.93	(1$\bar{1}\bar{1}$)	($\bar{1}\bar{1}\bar{1}$)	62.93
($\bar{1}$11)	($\bar{1}\bar{1}$1)	56.92	(1$\bar{1}\bar{1}$)	(1$\bar{1}$1)	56.92
($\bar{1}$11)	($\bar{1}$00)	62.44	(1$\bar{1}\bar{1}$)	(100)	62.44
($\bar{1}$11)	($\bar{2}$02)	47.53	(1$\bar{1}\bar{1}$)	(20$\bar{2}$)	47.53
($\bar{1}\bar{1}\bar{1}$)	($\bar{1}\bar{1}$1)	85.44	(111)	(1$\bar{1}$1)	85.44
($\bar{1}\bar{1}\bar{1}$)	($\bar{1}$00)	54.60	(111)	(100)	54.60
($\bar{1}\bar{1}\bar{1}$)	($\bar{2}$02)	86.15	(111)	(20$\bar{2}$)	86.15

X-ray pole figures confirm the chirality of the bulk films but provide no information on the chirality of the surface. One way to test the surface chirality is to study the enantiospecific electrooxidation of a chiral molecule in solution. Attard[11] has studied the electrochemical oxidation of sugars on chiral Pt surfaces, while Gellman et al.[44] have used temperature-programmed desorption (TPD) to study enantioselective desorption of chiral molecules from chiral metal surfaces. CuO electrodes have been shown to be catalytic for the electrooxidation of carbohydrates, amino acids, and amines with picomole sensitivity.[45−47] Xie and Huber[46] proposed a complex mechanism in which the CuO−analyte complex

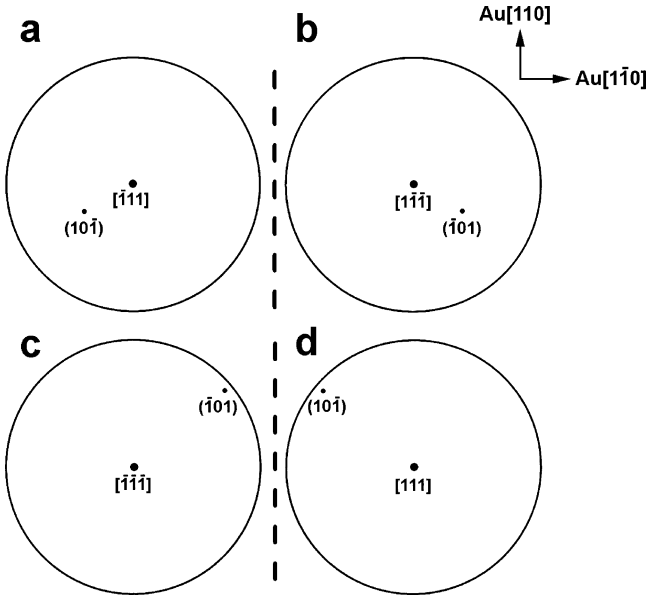

Figure 13. Stereographic projections for the (a) ($\bar{1}$11), (b) (1$\bar{1}\bar{1}$), (c) ($\bar{1}\bar{1}\bar{1}$), and (d) (111) orientations indicating the positions where the (10$\bar{1}$)-type reflections should be observed in the pole figures. The Au directions provide the reference for comparing the positions of observed reflections in pole figures for films grown from different enantiomers.

bridges with the adjacent CuO·OH active site to form a cyclic intermediate. The oxidation of this cyclic intermediate is reported to be the rate-limiting step. A smaller hydroxide concentration was expected to lower the catalytic efficiency. Labuda et al.[48] have reported increased sensitivity for the electrooxidation of amino acids with an increase in solution pH.

Chiral recognition of tartrate ion by the electrodeposited CuO on Au(001) was also demonstrated by electrochemical oxidation studies. Consistent with other studies, the electrochemical oxidation using chiral CuO films was carried out in a solution containing 5 mM tartaric acid in 0.1 M NaOH. The cyclic voltammograms (CV) were obtained in unstirred solutions by scanning from OCP to 0.75 V vs SCE at a scan rate of 10 mV/sec. Before switching solutions the electrode was cleaned by scanning in 0.1 M NaOH from the OCP to 0.75 V vs SCE to remove adsorbed remnants from the electrode. Figure 9a, b, and c show the cyclic voltammograms for the films grown in L-tartaric acid, D-tartaric acid, and DL-tartaric acid solutions, respectively, in 0.1 M NaOH and 5 mM D-tartaric acid or 5 mM L-tartaric acid solution. The scan in 0.1 M NaOH is a baseline scan which shows the onset potential for oxidation of water on a CuO electrode. Oxidation of water on CuO electrode occurs at approximately 0.6 V vs SCE. Figure 9a shows that the film grown from L-tartaric acid selectively oxidizes L-tartaric acid over D-tartaric acid. Figure 9b shows that the film grown from D-tartaric acid selectively oxidizes D-tartaric acid over L-tartaric acid. Figure 9c is a control experiment demonstrating that an achiral film shows no selectivity for the electrooxidation of tartaric acid.

For practical application of the CuO films for chiral synthesis, and sensing it would be preferred if substates

(44) Gellman, A. J.; Hovrath, J. D.; Buelow, M. T. *J. Mol. Catal. A* **2001**, *167*, 3.
(45) Wels, B.; Johnson, D. C. *J. Electrochem. Soc.* **1990**, *137*, 2785.
(46) Xie, Y.; Huber, C. O. *Anal. Chem.* **1991**, *63*, 1714.
(47) Kano, K.; Torimura, M.; Esaka, Y.; Goto, M. *J. Electroanal. Chem.* **1994**, *372*, 137.
(48) Labuda, J.; Meister, A.; Gläser, P.; Werner, G. *Fresenius' J. Anal. Chem.* **1998**, *360*, 654.

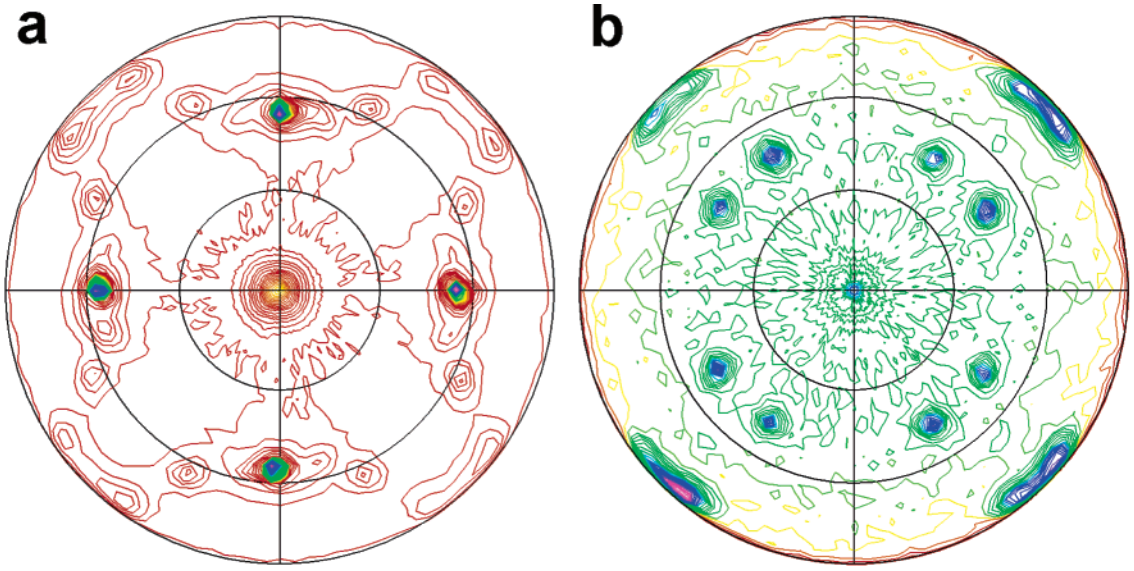

Figure 14. Pole figures probing the in-plane orientation for a CuO film on Au(001) grown from a solution of L-alanine using (a) (111) reflections and (b) (20$\bar{2}$) reflections.

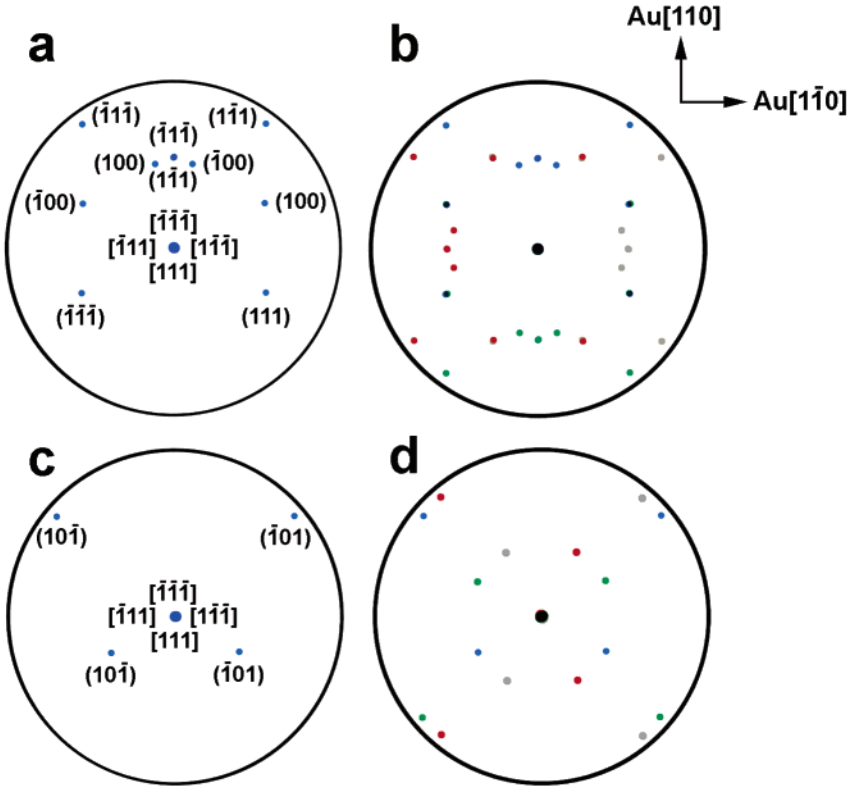

Figure 15. (a) Expected (111) pole figure obtained by overlaying the stereographic projections for the four orientations in Figure 12 under the assumption that only one domain of each orientation is deposited. (b) Expected (111) pole figure for four domains obtained by rotating part (a) by 90°, 180°, and 270° shown in gray, green, and red, respectively, and overlaying them. (c) Expected (20$\bar{2}$) pole figure obtained by overlaying the stereographic projections for the four orientations in Figure 13 under the assumption that only one domain of each orientation is deposited. (d) Expected (20$\bar{2}$) pole figure for four domains obtained by rotating part (a) by 90°, 180°, and 270° shown in gray, green, and red, respectively, and overlaying them.

less expensive than single-crystal Au could be used. We show in Figure 10 that CuO films deposited onto textured polycrystalline Au can also exhibit chiral recognition for the electrochemical oxidation of tartaric acid. The Au substrates were electrochemical quartz crystal microbalance (EQCM) electrodes comprised of thin vapor-deposited Au films on quartz substrates. The films have a [111] fiber texture but no in-plane order. Due to the lack of in-plane order for the Au films, it is not possible to use pole figure analysis to determine the orientation of the CuO films relative to the Au substrate. It may be possible in future work to use more localized techniques such as electron backscattered diffraction (EBSD) or TEM to determine the local orientation relationships. Figure 10a shows that the CuO film grown from L-tartaric acid selectively oxidizes L-tartaric acid over D-tartaric acid, while Figure 10b shows that the CuO film grown from D-tartaric acid selectively

Table 4. Enantiomeric Excesses for CuO Films Grown from Various Solution Precursors Determined from the (111)-Type Reflections

solution precursor	Major Orientation Type I (fraction) $(1\bar{1}\bar{1})$	$(\bar{1}11)$	enantiomeric excess Type I (%)	Major Orientation Type II (fraction) $(\bar{1}\bar{1}\bar{1})$	(111)	enantiomeric excess Type II (%)
L-tartaric acid	0.975	0.025	95	none	none	
D-tartaric acid	0.032	0.968	93	none	none	
DL-tartaric acid	0.50	0.50	0	none	none	
L-alanine	0.40	0.60	20	0.58	0.42	16
D-alanine	0.66	0.34	32	0.34	0.66	32
DL-alanine	0.49	0.51	2	0.50	0.50	0
L-valine	0.30	0.70	40	0.57	0.43	14
D-valine	0.76	0.24	52	0.38	0.62	24
DL-valine	0.50	0.50	0	0.51	0.49	2
glycine	0.50	0.50	0	none	none	

oxidizes D-tartaric acid over L-tartaric acid. Figure 10c is a control experiment demonstrating that an achiral CuO film deposited from racemic DL-tartaric acid shows no selectivity. Work is underway to determine whether chiral recognition on polycrystalline Au is caused by local chirality on individual Au grains, or if more global order is induced on the surface by the adsorbed molecules.

Deposition from Amino Acids. Films of CuO can also be deposited from alkaline solutions using amino acids to complex Cu(II) instead of tartaric acid. Polycrystalline films of CuO have been deposited from a solution of 5 mM $CuSO_4$ with excess amino acids (50 mM) in 0.2 M NaOH.[17] The same solution with the amino acids alanine, valine, and glycine as complexing agents was used in the present study to deposit films on an Au(001) single crystal. Alanine and valine are chiral, while glycine is achiral. The films on Au(001) substrates were deposited at 100 μA/cm^2 for 5 min.

Figure 11 shows the $\theta-2\theta$ X-ray diffraction scan of a CuO film grown using L-alanine as a complexing agent. The peaks at $2\theta = 35.57°$ ($d = 0.2524$ nm) and $2\theta = 38.74°$ ($d = 0.2322$ nm) indicate the presence of $\{\bar{1}11\}$ and $\{1\bar{1}\bar{1}\}$ out-of-plane orientations for the electrodeposited film. In contrast to the films grown from tartaric acid we see that two different orientations are evident in the X-ray diffraction scan. Table 2 lists the set of planes that have the same d-spacings. The $(1\bar{1}\bar{1})$, $(\bar{1}11)$, $(11\bar{1})$, and $(\bar{1}\bar{1}1)$ planes all have an identical d-spacing of 0.2524 nm, and it is impossible to distinguish between the orientations based on the $\theta-2\theta$ scans. Similarly, the (111), $(\bar{1}\bar{1}\bar{1})$, $(1\bar{1}1)$, and $(\bar{1}1\bar{1})$ planes all have a d-spacing of 0.2322 nm.

Figure 12a and b show the $(\bar{1}11)$ and $(1\bar{1}\bar{1})$ stereographic projections of monoclinic CuO while probing the (100) and (111)-type reflections. Figure 12a shows that for the $(\bar{1}11)$ orientation, reflections from the $(\bar{1}1\bar{1})$ plane at $\chi = 57°$ and the (111) plane at $\chi = 63°$ are separated azimuthally by 115° rotated clockwise ($\Delta\phi = +115°$). Figure 12b shows that for the $(1\bar{1}\bar{1})$ orientation, reflections from the $(1\bar{1}1)$ plane at $\chi = 57°$ and the $(\bar{1}\bar{1}\bar{1})$ plane at $\chi = 63°$ are separated azimuthally by 115° rotated counterclockwise ($\Delta\phi = -115°$). Figure 12a and b show that the stereographic projections of the $(1\bar{1}\bar{1})$ and $(\bar{1}11)$ planes are nonsuperimposable mirror images of each other. Figure 12c and d show the $(\bar{1}\bar{1}\bar{1})$ and (111) stereographic projections for monoclinic CuO while probing the (100) and (111)-type reflections. Figure 12c shows that for the $(\bar{1}\bar{1}\bar{1})$ orientation, reflections from the $(\bar{1}00)$ plane at $\chi = 55°$ and the $(\bar{1}1\bar{1})$ plane at $\chi = 85°$ are separated azimuthally by 49° rotated counterclockwise ($\Delta\phi = -49°$). Figure 12d shows that for the (111) orientation, reflections from the (100) plane at $\chi = 55°$ and the $(1\bar{1}1)$ plane at $\chi = 85°$ are separated azimuthally by 49° rotated clockwise ($\Delta\phi = +49°$). Figure 12c and d are nonsuperimposable mirror images of each other, i.e., the $(\bar{1}\bar{1}\bar{1})$ and (111) planes are enantiomers. The interplanar angles for these planes of interest are summarized in Table 3. This information is used to analyze the CuO(111) pole figure.

Figure 13 shows the stereographic projections for the (a) $(\bar{1}11)$, (b) $(1\bar{1}\bar{1})$, (c) $(\bar{1}\bar{1}\bar{1})$, and (d) (111) orientations while probing the $(10\bar{1})$-type reflections for monoclinic CuO. The interplanar angles for these planes of interest are summarized in Table 3. In Figure 13a and b, the peaks at $\chi = 47°$ are assigned to the $\{10\bar{1}\}$ and $\{\bar{1}01\}$ reflections for CuO$(\bar{1}11)$ and CuO$(1\bar{1}\bar{1})$ orientations, respectively. Similarly, in Figure 13c and d, the peaks at $\chi = 86°$ are assigned to the $\{\bar{1}01\}$ and $\{10\bar{1}\}$ reflections for CuO$(\bar{1}11)$ and CuO(111) orientations, respectively. Figure 13a and d show that the $(10\bar{1})$ reflection for the $(\bar{1}11)$ orientation appears at $\phi = 240°$, while the same reflection for the (111) orientation appears at $\phi = 310°$. Similarly, Figure 13b and c show that the $(\bar{1}01)$ reflection for the $(1\bar{1}1)$ and $(\bar{1}\bar{1}\bar{1})$ orientations appear at $\phi = 120°$ and $\phi = 50°$, respectively.

Figure 14a and b show the CuO(111) and CuO$(20\bar{2})$-pole figures for the film deposited from a L-alanine solution. As discussed earlier, the CuO(111) pole figure shown in Figure 14a is actually a superposition of CuO(111), Au(111), and CuO(100) pole figures. The reflections at $\chi = 63°$ from the domains due to the $(\bar{1}11)$ and the $(1\bar{1}\bar{1})$ orientations obtained from the amino acid solution give results similar to that obtained for the tartrate complexed films discussed earlier in the paper, albeit with reduced enantioselectivity. The low intensity peaks to the left ($\Delta\phi = -12.5°$ from the nearest Au peak) and right ($\Delta\phi = 12.5°$ from the nearest Au peak) of the intense Au peaks at $\chi \approx 55°$, result from the (100)-type reflections, as indicated by the stereographic projections shown in Figure 12c and d. Additional peaks at $\chi \approx 85°$ can be attributed to the reflection of (111)-type planes. The peaks at $\Delta\phi = +115°$ from the Au(111) peaks in Figure 14a are slightly more intense than the peaks at $\Delta\phi = -115°$ suggesting that the film grown from L-alanine solution has a slight excess of the $(\bar{1}11)$ orientation. In contrast to the films grown from pure L-tartaric acid or pure D-tartaric acid which have four equal intensity peaks at $\chi = 63°$, the films grown from pure alanine enantiomers have eight peaks at $\chi = 63°$.

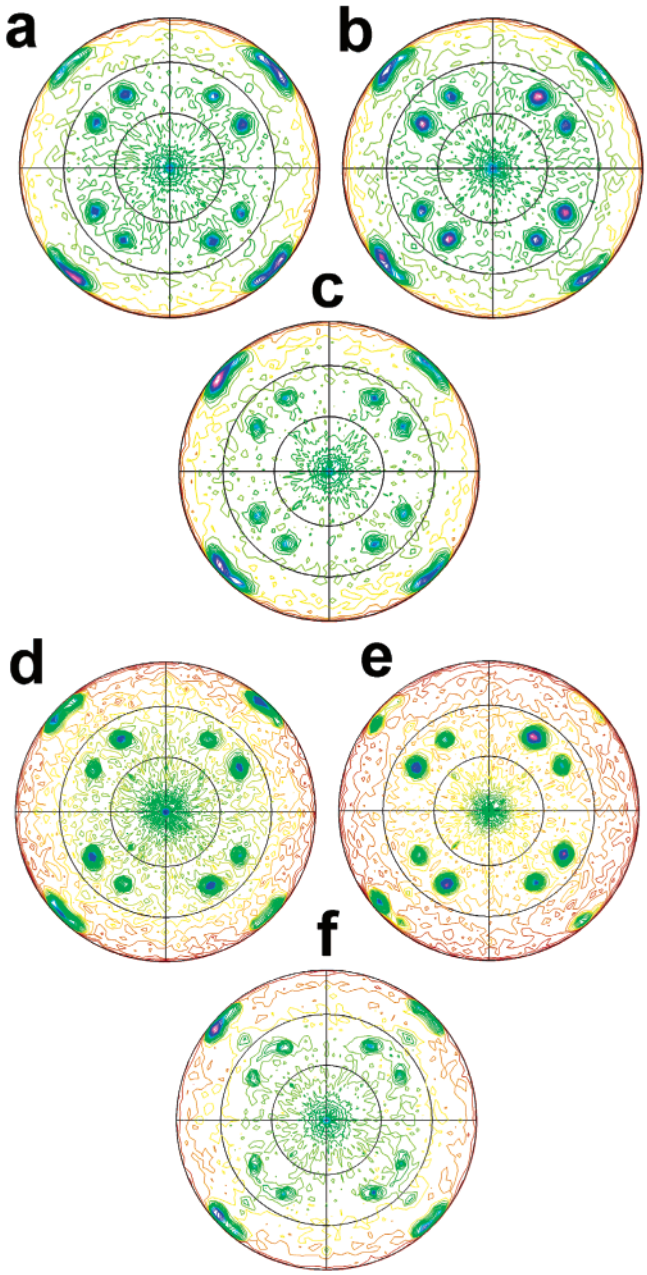

Figure 16. CuO($20\bar{2}$) pole figures for various CuO films grown on Au(001) from solutions of (a) L-alanine, (b) D-alanine, (c) DL-alanine, (d) L-valine, (e) D-valine, and (f) DL-valine. The pole figures for films grown from L-alanine and L-valine solution have a small excess of the chiral ($\bar{1}11$) and ($\bar{1}\bar{1}\bar{1}$) orientations. The films grown from D-alanine and D-valine have a small excess of ($1\bar{1}\bar{1}$) and (111). The films grown from racemic mixtures of alanine and valine show no enantiospecificity for any chiral orientations.

Although the ($\bar{1}11$) orientation is slightly preferred over the ($1\bar{1}\bar{1}$), the figure resembles the results obtained for DL-tartaric acid films. This will be elucidated further later in the text. Similarly, the film grown from L-alanine solution seems to have a small preference for the ($\bar{1}\bar{1}\bar{1}$) orientation but it is rather difficult to justify decisively based on the weak signal-to-noise ratio at high tilt angles and the overlapping of {100} reflections with the Au peaks at $\chi = 55°$.

The (111) pole figure, although very complicated, is useful because it provides an internal reference in the form of Au peaks at $\chi = 55°$, which aid in comparing and determining the chiral orientations in conjunction with the stereographic projections. A simpler pole figure is obtained by probing the CuO($20\bar{2}$) reflection. A CuO($20\bar{2}$) pole figure is run by fixing the 2θ to the d-spacing of the CuO($20\bar{2}$) reflection. The resulting pole figure shown in Figure 14b is simple compared with the CuO(111) pole figure but it fails to provide an internal reference to determine the precise chiral orientation. The Au[110] direction at $\phi = 0°$ is used as the reference. The peaks at $\chi = 48°$ and $\chi = 86°$ are due to the ($10\bar{1}$)-type reflections for the four different orientations.

The analysis of the (111) pole figure can be verified by overlaying the stereographic projections for the four orientations in Figure 12. The resulting figure is shown in Figure 15a, assuming that only one domain of each orientation is deposited. But Au(001) is a 4-fold symmetric surface so it is reasonable to expect four domains of each orientation being deposited on the surface. The resultant image with four domains of each orientation obtained by rotating Figure 15a by 90°, 180°, and 270° and overlaying them is shown in Figure 15b. The gray, green, and red spots signify different domains obtained by rotating Figure 15a by 90°, 180°, and 270°, respectively. Identical analysis for the ($20\bar{2}$) pole figure is shown in Figure 15c and d. The resultant figures shown in Figure 15b and d match the experimentally observed pole figures shown in Figure 14a and b, respectively. The results of CuO(111) and CuO($20\bar{2}$) pole figures show that the film has four different chiral orientations with four domains of each orientation.

Figure 16 shows the CuO($20\bar{2}$) pole figures for various CuO films grown from solutions of (a) L-alanine, (b) D-alanine, (c) DL-alanine, (d) L-valine, (e) D-valine, and (f) DL-valine. The pole figures show that the films grown from L-alanine and L-valine solutions have an excess of chiral ($\bar{1}11$) and ($\bar{1}\bar{1}\bar{1}$) orientations compared to their mirror image counterparts, the ($1\bar{1}\bar{1}$) and (111) orientations, respectively. Similarly the films grown from D-alanine and D-valine have an excess of ($1\bar{1}\bar{1}$) and (111) compared to their mirror image counterparts ($\bar{1}11$) and ($\bar{1}\bar{1}\bar{1}$), respectively. The films grown from racemic mixtures of alanine and valine show no enantiospecificity for any chiral orientations. Approximately equal distributions of the ($\bar{1}11$) and ($1\bar{1}\bar{1}$) orientations and the (111) and ($\bar{1}\bar{1}\bar{1}$) orientations are observed in the pole figures. Although not shown, pole figures obtained for films grown from achiral glycine as a complexing agent have equal amounts of the chiral CuO($\bar{1}11$) and CuO($1\bar{1}\bar{1}$) orientations.

The enantiomeric excesses were determined from the azimuthal scans by probing the (111)-type reflections for the chiral orientations. The results obtained for films grown from tartaric acid and various amino acids are summarized in Table 4. In contrast to the films grown from pure L-tartaric acid and pure D-tartaric acid which have high ee for ($1\bar{1}\bar{1}$) and ($\bar{1}11$) orientations respectively, the films grown from pure enantiomers of amino acids show lower ee for the two chiral orientations.

It was argued earlier in this article that the adsorption of the solution precursor on the Au(001) surface is an important factor governing the observed orientation. Although formation of extended surface chirality[41,44] is desired, it is not always the case. Studies on adsorption of organic molecules on surfaces have revealed forma-

tion of local chiral domains or local chiral imprinting without yielding extended surface chirality.[40,49,50] Energies for the adsorption of D- and L-glucose on chiral Pt(643) have been shown to differ by only 1.2 kJ/mol,[51] while the difference in the adsorption energies of two enantiomers of methylcyclohexanone on chiral Cu(643) surfaces have been shown to differ by only 0.9 kJ/mol.[44] Adsorption of (*R*, *R*)-tartaric acid on Cu(110) is reported to reconstruct the Cu surface to form two chiral domains differing in energies by 6 kJ/mol.[42] While a great deal of attention has been focused on the adsorption of chiral amino acids on Cu[52,53] single crystals, similar studies on Au single crystals are limited. Adsorption of amino acids on Au[54] and Ag[55] surfaces are reported to be physical in nature,[56] while amino acids chemisorb on Cu single crystals. Cysteine is known to adsorb on Au,[57] but the high affinity of Au for sulfur groups is widely used to form self-assembled monolayers on gold.[58] Based on the argument that weak adsorption of amino acids on Au as compared to tartaric acid results in the formation of disoriented films, CuO films deposited on Cu single crystals from amino acid solution should be more ordered. Indeed, in recent unpublished work[59] we have shown that CuO films with just one chiral orientation are deposited on Cu(111) single crystals from identical amino acid solutions used in this study.

Films of CuO electrodeposited onto Au(001) from the amino acids can also be used for chiral recognition. Surprisingly, the films deposited from amino acids are enantioselective for the electrochemical oxidation of tartaric acid, but not for the electrochemical oxidation of amino acids. Films deposited from D-amino acids are enantioselective for the oxidation of L-tartaric acid, while films deposited from L-amino acids are enantioselective for the oxidation of D-amino acids. Films deposited from DL-amino acids or from achiral glycine show no enantioselectivity.

Conclusions

Chiral films of CuO were deposited on Au(001) single-crystal surfaces from alkaline solutions of Cu(II) complexes of tartaric acid and the amino acids alanine, valine, and glycine. The films produced from tartaric acid deposit with the enantiomeric $(\bar{1}11)$ and $(1\bar{1}\bar{1})$ orientations. L-Tartaric acid produces the $(1\bar{1}\bar{1})$ orientation with 95% ee, while D-tartaric acid produces the $(\bar{1}11)$ orientation with 93% ee. Chiral recognition of tartaric acid was demonstrated using cyclic voltammetry. CuO deposited from L-tartaric acid selectively oxidizes L-tartaric acid over D-tartaric acid, while CuO deposited from D-tartaric acid selectively oxidizes D-tartaric acid over L-tartaric acid. A film of CuO deposited from DL-tartaric acid which has equal amounts of the $(\bar{1}11)$ and $(1\bar{1}\bar{1})$ orientations shows no enantiospecificity in the cyclic voltammetric experiments.

Films deposited from the chiral amino acids alanine and valine grow with two types of orientations, each of which has a lower ee than the films deposited from tartaric acid. The type I orientation consists of the $(\bar{1}11)$ and $(1\bar{1}\bar{1})$ pair, while the type II orientation consists of the $(\bar{1}\bar{1}\bar{1})$ and (111) pair. The planes in each of these pairs are nonsuperimposable mirror images of each other. The type I orientations are produced from the amino acids with the opposite hand to those produced from tartaric acid. That is, L-alanine and L-valine produce an excess of the $(\bar{1}11)$ orientation, while D-alanine and D-valine produce an excess of the $(1\bar{1}\bar{1})$ orientation. For the type II orientation, the L-enantiomers of the amino acids produce an excess of the $(\bar{1}\bar{1}\bar{1})$ orientation, while the D-enantiomers produce an excess of the (111) orientation. Films of CuO deposited from a solution of the achiral amino acid glycine consist of a racemic mixture of the $(\bar{1}11)$ and $(1\bar{1}\bar{1})$ orientations. Although the mechanism of enantiospecific electrodeposition is not known, it is speculated that the symmetry of the Au(001) surface is broken by the adsorption of chiral solution precursors.

Acknowledgment. This work was supported by National Science Foundation grants CHE-0243424, CHE-0437346, DMR-0071365, and DMR-0076338, and Department of Energy grant DE-FC07-03ID14509.

CM048939X

(49) Lopinski, G. P.; Moffat, D. J.; Wayner, D. M.; Wolkov, R. *Nature* **1998**, *39*, 909.
(50) Vishwanathan, R.; Zazadzinski, J. A.; Schwartz, D. K. *Nature* **1994**, *368*, 440.
(51) Attard, G. A.; Ahmadi, A.; Feliu, J.; Rodes, A.; Herrero, E.; Blais, S.; Jerkiewicz, G. *J. Phys. Chem. B* **1999**, *103*, 1381.
(52) Williams, J.; Haq, S.; Raval, R. *Surf. Sci.* **1996**, *368*, 303.
(53) Chen, Q.; Lee, C. W.; Frankel, D. J.; Richardson, N. V. *Phys. Chem. Commun.* **1999**, 9.
(54) Zhao, X.; Yan, H.; Zhao, R. G.; Yang, W. S. *Langmuir* **2002**, *18*, 3901.
(55) Zhao, X.; Yan, H.; Tu, X.; Zhao, R. G.; Yang, W. S. *Langmuir* **2003**, *19*, 5542.
(56) Lange, W.; Jirikowsky, M.; Benninghoven, A. *Surf. Sci.* **1984**, *136*, 419.
(57) Di Felice, R.; Selloni, A.; Molinari, E. *J. Phys. Chem. B* **2003,** *107,* 1151.
(58) Ulman, A. *Chem. Rev.* **1996**, *96*, 1533.
(59) Bohannan, E. W.; Kothari, H. M.; Nicic, I. M.; Switzer, J. A. Unpublished work.